Elastic Properties of a Single Lamella of Montmorillonite by Molecular Dynamics Simulation

Oleg L. Manevitch and Gregory C. Rutledge*

Department of Chemical Engineering, Massachusetts Institute of Technology, Cambridge, Massachusetts 02139

Received: February 28, 2003; In Final Form: September 16, 2003

We present results for the elastic properties of a single lamella of montmorillonite consisting of two tetrahedral layers and the intervening octahedral layer. The calculations were performed using a force field with both bonded and nonbonded interatomic contributions and periodic boundary conditions in two dimensions, representing an infinite "nanoplate". The elastic response of the atomically thin nanoplate was calculated from curves of force versus displacement obtained at slow rates of deformation. Bending stiffness was estimated independently from the onset of nonlinear deformation under compression. The atomistic results are explained in terms of a continuum model for thin plates. We obtain values for the in-plane elastic properties of 250−260 N/m for E_1h and E_2h, and 166 N/m for the in-plane shear response, G_3h, where h is the thickness of the nanoplate. The effective mechanical thickness of the clay lamella is found to be 0.678 nm, comparable to the distance between the outermost layers of atoms on either surface of the atomically thin sheet (0.615 nm). A bending modulus of 1.25×10^{-17} Nm is obtained from the critical stress for nonlinear compression.

1. Introduction

Nanocomposites are a new class of composite materials comprised of a polymer matrix filled with particles, rods, or plates having at least one dimension on the nanometer length scale. Polymer−clay nanocomposites in particular have received considerable attention recently.[1] Understanding the mechanical performance of these materials requires, in particular, the knowledge of the properties of nanoparticles themselves. In exfoliated clay nanocomposites, the particulate material may be individual dispersed lamellae of clay having a thickness on the order of 1 nm and lateral (in-plane) dimensions of 100−1000 nm. Such high aspect ratios are generally advantageous for a number of composite properties, among them mechanical reinforcement and barrier properties. When one of the dimensions of such particles is of atomic length scale, the question arises as to the applicability of traditional concepts of macroscopic solids and the continuum mechanics thereof.[2] Because it is difficult to measure the mechanical properties of such nanoplates directly by experimental means, computer simulation is the best available method for exploring this question and for providing estimates of the mechanical properties of individual nanoplates.

For the particular case of clay-based nanoparticles, the situation is very similar to a thin plate because the ratio of thickness to the in-plane dimensions is much less than unity. Under these conditions, the continuum mechanical theory for thin plates implies the following: (1) infinitesimal deformation of the plate can be considered as a superposition of a plane stress state (calculated from equations of equilibrium averaged by thickness) and transverse bend−twist deformation, and (2) during transverse deformation the normal displacements in cross-section as well as normal strains and stresses vary linearly in the thickness direction. These results for continuum mechanics are readily obtained within the framework of a three-dimensional theory by using perturbation expansions, where the small

parameter is the ratio of thickness (h) to the in-plane size of the plate (L). Using these results, one can further show that under bending conditions the ratio of in-plane shear stress to in-plane tensile stress is of the order of h/L. The magnitude of normal (i.e., out-of-plane) stress, in the case of bending of a thin plate with free z-boundaries or one loaded z-boundary, is also much smaller than those for transverse shear stresses, their ratio being also of the order of h/L. So, the most important components of the stress state for a thin plate are the in-plane tensile (σ_1, σ_2) and in-plane shear (σ_6) stresses, determined by the equations of plane stress state for the case of loading within the plane of the lamina, and the in-plane tensile stresses (σ_1, σ_2) which vary linearly in the z-direction for the case of transverse loading.

Molecular dynamics simulation has been applied successfully to different problems of thermodynamics and mechanics of clay minerals.[3−8] Seo et al.[7] used molecular dynamics to compute the elastic constants of bulk quartz, albite and muscovite, with good results. Sato et al. performed molecular dynamics simulations of a single layer of beidellite under compression.[8] Their work suggests that clay sheets may bend under compressive strains up to 40% before failure, with stresses on the order of 0.7 GPa; however, they did not report any values for mechanical properties such as elastic constants. Thus, despite great current interest in montmorillonite (MMT), there remains a dearth of information regarding the detailed structure and mechanical properties of isolated clay sheets. The calculation of these is the main goal of this paper. Our results are then compared to data for other silicates and oxides of alumina.[9,10]

2. Method

2.1. Model Development. The model under consideration was a single clay sheet of MMT, that is, a clay lamella composed of one crystallographic unit cell in the thickness direction and an infinite number of unit cells in the two in-plane directions. The general formula for the class of MMTs is $(Na,Ca)_{0.33}$-$(Al_{2-y},Mg_y)Si_4O_{10}(OH)_2 \cdot nH_2O$. The crystal structure is mono-
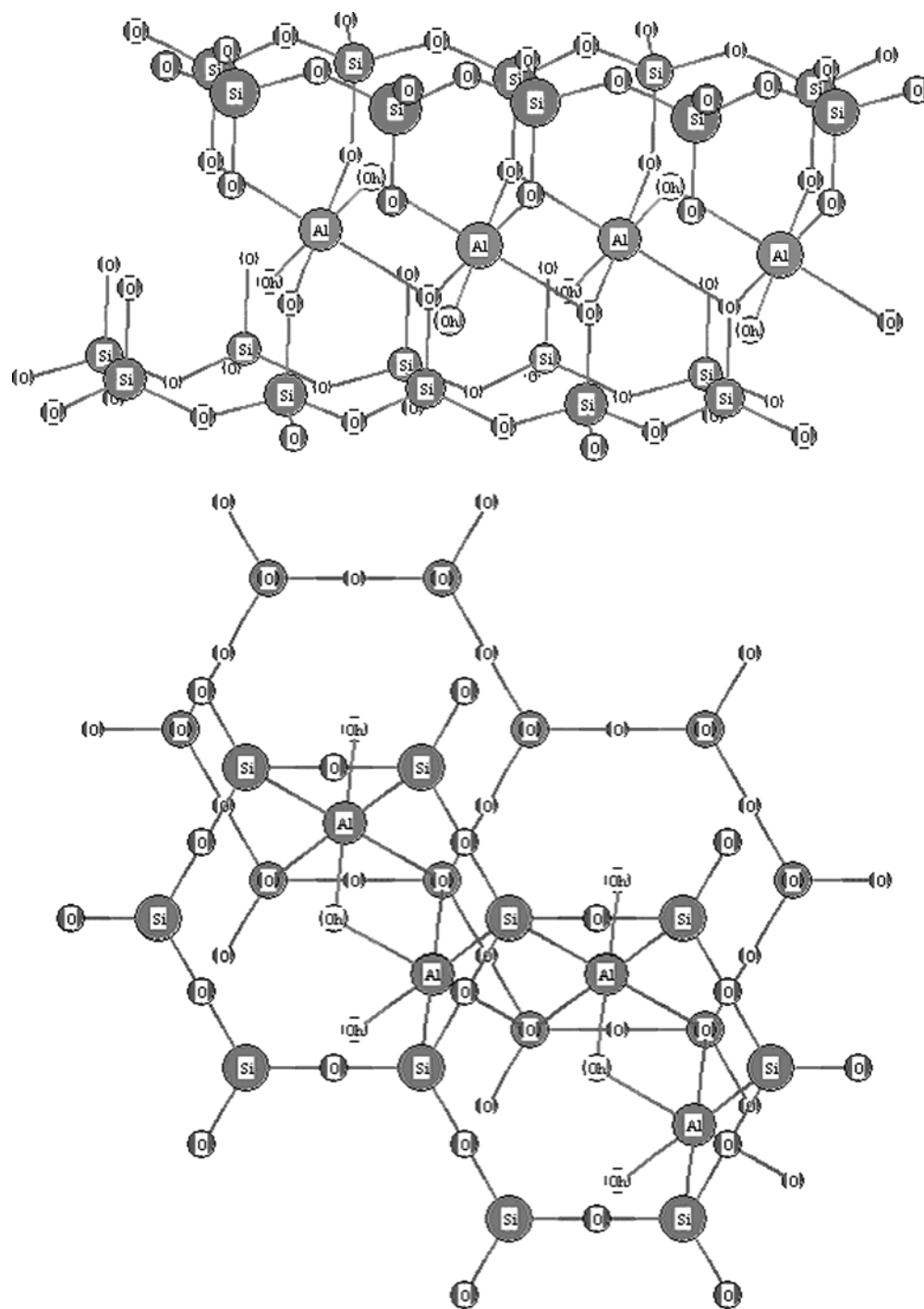
Figure 1. Crystal structure of montmorillonite: (a) the view along the *b*-axis; (b) the view normal to the *ab*-plane.

clinic with $a = 0.53$ nm, $b = 0.92$ nm, $\beta = 97°$. The value of c depends on the size of the galleries between two neighboring laminas and varies greatly among members of this class of silicates.[9] Many interesting properties of such silicates are due to their capacity for substitution of various atoms in octahedral and tetrahedral sheets. These substitutions include Al^{3+} by Mg^{2+} in the octahedral sheet, together with Si^{4+} by Al^{3+} in the tetrahedral sheet, and result in a net negative charge on the sheet. The negative charge imbalance is neutralized by adsorption of exchangeable cations between the clay sheets. In this work, we consider the neutral MMT structure, that is, without substitutions or absorbed cations (Figure 1). The corresponding chemical formula is $[Al_2Si_4O_{10}(OH)_2]_2$ for the unit cell.

Despite the monoclinic crystal symmetry, we expect the elastic properties of the clay sheet to be approximately ortho-

tropic. This has the advantage of reducing the number of elastic constants required to characterize the sheet. To check the validity of this approximation, it is necessary to examine well-known relations between the moduli of elasticity and Poisson's coefficients that have to be satisfied in the orthotropic case.

Our computational algorithm for generating the initial structure for the MMT crystal was devised to reflect as closely as possible the coordinates of atoms within the unit cell, reported in ref 9, while satisfying orthotropic boundaries of the simulation cell for the purpose of defining stresses and strains. The initial configuration was constructed in two stages. First, a number of unit cells were replicated in space to create a crystal sheet larger than the intended simulation box. Then, the part of the crystal corresponding to a simulation cell with orthotropic boundaries was extracted and periodic boundary conditions were applied

TABLE 1: Parameters for the Force Field Used in This Work[a]

	l_0, θ_0	k_b, k_θ	mass (g/mole)[e]	ϵ	σ	z^e
Si−O[b,d]	0.1665	39 280	na	0.095 52	0.3822	na
Al−O[b,d]	0.1775	39 280	na	1.436	0.3072	na
Si−Si[d]	na	na	28.086	0.040 01	0.4550	+4
Al−Al[d]	na	na	26.982	9.043	0.2941	+3
O−O[d]	na	na	16.000	0.2280	0.3210	−2
Si−Al[d]	na	na	na	0.6016	0.3658	na
Si−O−Si[c]	149.8	31.1	na	na	na	na
O−Si−O[c]	113.1	42.3	na	na	na	na
O−Al−O[c]	113.1	42.3	na	na	na	na
Al−O−Al[c]	149.8	31.1	na	na	na	na
Si−O−Al[c]	149.8	31.1	na	na	na	na

[a] Entries of "na" indicate "not applicable". [b] Bond stretch potential between bonded atom pairs: $E = k_b(l - l_0)^2$; l_0 in nm, k_b in kcal/mol/nm². [c] Angle bending potential: $E = k_\theta(\theta - \theta_0)^2$; θ in deg, k_θ in kcal/mol/deg². [d] The van der Waals contribution to the interatomic nonbonded interaction potential: $E_{vdw} = \epsilon[(\sigma/r)^{12} - 2(\sigma/r)^6 - (\sigma/r_{cut})^{12} + 2(\sigma/r_{cut})^6]$ for $r < r_{cut}$, and $E_{vdw} = 0$ otherwise.; ϵ in kcal/mol, σ in nm. The Coulombic contribution to the interatomic nonbonded potential: $E_c = z_i z_j e^2/4\pi\epsilon_o r$; e is the electron charge and ϵ_o is the vacuum dielectric. [e] Atomic masses and charges are tabulated with the corresponding pairwise interaction between like atoms.

in the in-plane directions to avoid additional free surfaces. During subsequent molecular dynamics simulation, both the coordinates of the atoms and the dimensions of the simulation cell were allowed to equilibrate according to the chosen interaction potential, as described in the next section.

2.2. Molecular Dynamics Simulation. The system was simulated by molecular dynamics (MD) using a program originally derived from Puma[11] and modified to take advantage of the array syntax in Fortran 90. For most of our calculations, the computational cell consisted of 288 atoms arranged in an array of four by two unit cells. These form a parallelepiped with initial dimensions $L_X = 2.18$ nm and $L_Y = 1.88$ nm. Periodic boundary conditions were used to create an infinite sheet in the *x*- and *y*-directions. In the *z*-direction, the periodic boundary was set at 4 nm, large enough to preclude any significant interaction between the simulated clay sheet and its image. To check for system size effects, we also considered a computational cell of 648 atoms arranged in six by three unit cells.

The empirical force field reported in Table 1 was used to compute the energy of the system. This force field is based on the consistent valence force field (CVFF),[12] which includes harmonic bond-stretching and bond-angle-bending terms, a shifted 12−6 Lennard-Jones potential for nonbonded interactions, and a Coulombic term for interactions between atom-centered partial atomic charges. A cutoff of $R_{cut} = 1.05$ nm was used for the 12−6 nonbonded interactions. Coulombic interactions were calculated using Ewald sums,[13] modified to work with noncubic cells. For simplicity, we have collapsed the OH groups into single particles with mass and charge corresponding to the sum of the O and H values. We did not consider any special terms for hydrogen bonding.

The simulations were performed in either an *NzT* (constant displacement, constant temperature) or an *NfT* (constant force, constant temperature) ensemble for an atomically thin plate with periodic boundaries in two dimensions. These are analogous to the *NϵT* (constant strain, constant temperature) and *NσT* (constant stress, constant temperature) ensembles familiar for systems with periodic boundaries in three dimensions, used to represent bulk materials. Where periodic boundaries render the specification of length or cross-sectional area unambiguous,

displacement and force are readily converted to strain and stress. However, stress and strain requiring specification of the magnitude of the third, nonperiodic dimension are not prescribed unambiguously, and for this reason displacement and force descriptors are retained explicitly in the following exposition. The method of collisional dynamics method[14,15] ($f = 10$ ps⁻¹) was used to maintain isothermal conditions, and Berendsen's barostat ($m = 0.1$ au, $\beta_p = 0.014$ kbar⁻¹ ps⁻¹) was used to maintain constant stress.[16] Corrections were applied to prevent the rotation and translation of the system as a whole. The integration time step was 0.001 ps. The calculations were performed on a Pentium III 1 GHz computer.

3. Results

3.1. Equilibrium Structure. The system of 288 atoms was first equilibrated at 300 K for 10 ps under conditions of zero applied force ($f_x = f_y = f_z = 0$). A summary of the contributions from each of the energy terms is presented in Table 2. One estimate of the thickness of the plate h can be obtained from the distance between the two planes of oxygen atoms at either surface of the sheet. At a temperature of 300 K, this structurally defined average thickness h_s is computed to be 0.615 nm, in close agreement with the estimated value of 0.645 nm[9] for a single sheet (without galleries). The equilibrium structure of the simulated MMT sheet is in good agreement with data on bulk MMT.[10]

3.2. Deformation. The number of independent elastic constants for a system having orthotropic symmetry is nine, defined by eq 1:

$$\epsilon_1 = \frac{S_{11}}{h}\left(\frac{f_{xx}}{L_y}\right) + \frac{S_{12}}{h}\left(\frac{f_{yy}}{L_x}\right) + S_{13}\sigma_3$$

$$\epsilon_2 = \frac{S_{21}}{h}\left(\frac{f_{xx}}{L_y}\right) + \frac{S_{22}}{h}\left(\frac{f_{yy}}{L_x}\right) + S_{23}\sigma_3$$

$$\epsilon_3 = \frac{S_{31}}{h}\left(\frac{f_{xx}}{L_y}\right) + \frac{S_{32}}{h}\left(\frac{f_{yy}}{L_x}\right) + S_{33}\sigma_3 \quad (1)$$

$$\epsilon_4 = S_{44}\sigma_4$$

$$\epsilon_5 = S_{55}\sigma_5$$

$$\epsilon_6 = \frac{S_{66}}{h}\left(\frac{f_{xy}}{L_y}\right) = \frac{S_{66}}{h}\left(\frac{f_{yx}}{L_x}\right)$$

In terms of Young's moduli, shear moduli, and Poisson's ratios, these elastic compliance constants become

$$\frac{S_{ii}}{h} = \frac{1}{E_i h} \quad \text{for} \quad i = 1, 2, 3$$

$$\frac{S_{ij}}{h} = -\frac{\nu_{ij}}{E_j h} \quad \text{for} \quad j = 1, 2, 3; i \neq j \quad (2)$$

$$\frac{S_{ii}}{h} = \frac{1}{G_{i-3} h} \quad \text{for} \quad i = 4, 5, 6$$

In this work, we equate the 1, 2, and 3 directions (Voigt notation) with the *x*, *y*, and *z* Cartesian axes. The *x*- and *y*-axes correspond to the *a* and *b* directions of the MMT unit cell, respectively, whereas the *z*-axis is normal to the clay sheet. We can realize uniaxial extension or compression in the plane of the sheet (i.e., *x*- and *y*-directions) simply by changing the periodicity of the cell in these directions in accordance with

Elastic Properties of Montmorillonite

J. Phys. Chem. B, Vol. 108, No. 4, 2004 **1431**

TABLE 2: System Characteristics at Equilibrium for $N = 288$[a]

kinetic energy (kcal/mol)	257
bond-stretching energy (kcal/mol)	1123(27)
bond-angle-bending energy (kcal/mol)	7 165(13)
12−6 nonbonded interaction energy (kcal/mol)	−370(2)
Coulombic energy (kcal/mol)	−100 883(45)
total energy (kcal/mol)	−92 707(64)
stress σ_X (GPa)	−0.003(0.08)
stress σ_Y (GPa)	−0.002(0.07)
stress σ_Z (GPa)	−0.222(0.14)
density (g/cm³)	3.831(0.006)
L_X (nm)	2.1394(0.0017)
L_Y (nm)	1.9159(0.0014)

[a] Values in parenthesis are standard deviations.

the relation $x' = (1 + \epsilon_i)x$, where ϵ_i is the strain. Deformation at constant strain rate is accomplished by changing the size of the simulation cell by small amounts at successive time steps of the simulation, up to a limiting (low) value of total strain. In such a case it is necessary to be sure that the strain rate is sufficiently low that further decreases in strain rate do not alter the results. This can be shown to be the case for strain rates less than the velocity of sound in the material. By imposing an extension or compression, ϵ_1, in the x-direction and allowing the y- and z-dimensions of the sheet to relax (i.e., f_{yy} and f_{zz} are zero), we can calculate the elastic property E_1h and Poisson coefficient ν_{21} directly from the resulting force per unit length (f_{xx}/L_y) and strain ϵ_2 which develop. Analogously, deformation ϵ_2 in the y-direction allows us to calculate E_2h and ν_{12}. Finally, combined extension in the x-direction and compression in the y-direction while maintaining constant area leads to pure shear deformation on axes rotated 45° with respect to the x- and y-axes and allows calculation of the in-plane shear property. From the similarity of tensile properties observed in the x- and y-directions (see below), we equate this shear response with G_3h.

To determine elastic properties normal to the MMT sheet, it is necessary to define a loading plane. Because the sheet is atomically thin in this direction, this is not trivial. We have chosen to impose tensile deformation normal to the sheet by applying forces of equal magnitudes but opposite directions to all the oxygen atoms located at each surface of the sheet, in accord with a desired stress σ_3. The resulting displacement of one surface plane of oxygen atoms relative to the other surface plane was calculated, as well as normal strains ϵ_1 and ϵ_2. In this manner, we determined the elastic property E_3h and Poisson ratios ν_{13} and ν_{23} analogously to the in-plane elastic constants. Similarly, the shear properties G_1h and G_2h were calculated by loading the planes of oxygen atoms on either surface of the clay sheet with forces of equal magnitude but opposite direction. These forces were increased at a constant rate to achieve larger strains. We calculated the corresponding shear deformations using averaged coordinates for the oxygen atoms at the two free surfaces. It should be noted that the method used to determine E_3h, G_1h, G_2h, ν_{31}, and ν_{32} is less reliable than that used for the other elastic constants, but this turns out to be of little consequence because they do not play a significant role in the mechanical behavior of a thin plate. In all calculations the time-averaged forces and resulting stresses were calculated using the atomic virial.

3.3. Calculation of Elastic Properties for the Two-Dimensional Orthotropic Model. Results for a typical deformation (in the x-direction, in this case) at a strain rate of 1.5×10^{-3} m/s are shown in Figures 2−4. From the slopes of these curves, values for E_1h, ν_{12}, and ν_{13} are obtained. Values for these and the other elastic constants associated with in-plane

deformation are shown in Table 3. Similar results are obtained for a strain rate as high as 2×10^{-3} m/s; these are also reported in Table 3. Values are also reported in Table 3 for E_3h, ν_{31}, ν_{32}, G_1h, and G_2h obtained by applying forces to the oxygens in the surface planes of the MMT sheet. For values of h on the order of 1 nm, the values of G_1 and G_2 must be relatively large, substantiating the assumption of a two-dimensional (2D) orthotropic model, because the shear strains should be much smaller than rotations which occur under bending under this assumption.

The validity of the approximation of 2D orthotropicity for the MMT sheet can be further tested by how well the corresponding relations $E_i\nu_{ij} = E_j\nu_{ji}$ are satisfied. For $i = 1$, $j = 2$ (in-plane deformation) we obtain agreement to within 10%. From the simulated deformation normal to the sheet ($i = 3$, $j = 1$ or 2), the other two relations are not satisfied to such good accuracy. From this, we conclude that the assumption of orthotropic symmetry for the sheet is accurate only for in-plane and bend−twist deformations, but these are the important deformation modes for thin plates.

3.4. Determination of Bending Stiffness D_2. From the theory of thin plates, we can estimate the magnitudes of bending and torsion constants divided by the square of the sheet thickness for a single sheet of MMT from the deformations reported above:[17]

$$\frac{D_1}{h^2} = \frac{E_1h}{12(1 - \nu_{12}\nu_{21})}, \quad \frac{D_2}{h^2} = \frac{E_2h}{12(1 - \nu_{12}\nu_{21})}, \quad \frac{D_3}{h^2} = \frac{G_3h}{12} \quad (3)$$

These values are reported in Table 3. In addition, we performed an independent determination of the bending stiffness D_2 by imposing a compression of the plate along the y-direction; for sufficiently large compressive loads, the instability of the cell to bending may be observed. Because long wavelength bending modes are most unstable, it is necessary to construct a simulation cell that is large in the direction of compressive loading for most accurate results. For this purpose, we used a simulation cell having 576 atoms arrayed in 2 unit cells in the x-direction and 8 unit cells in the y-direction ($L_X = 1.088$ nm, $L_Y = 7.535$ nm) and a second simulation cell having 864 atoms arrayed in 2 by 12 unit cells ($L_x = 1.088$ nm, $L_y = 11.3$ nm). As a control, the original simulation cell with $N = 288$ was also investigated under compression with the same strain rate, to establish the upper limit for linear elasticity. During an MD simulation, the y-dimension of the simulation cell was compressed at a rate of 1.5×10^{-2} m/s for a period of 260 ps. For the cell with $N = 576$, the observed force per unit length f_{yy}/L_x is shown in Figure 5. The slope of this force versus strain response is shown in Figure 6. The initial slope of 252 N/m is in good agreement with the values for E_2h reported in Table 3.

The critical compressive load for a thin bar can be found in accordance with Euler's formula:

$$f_{yy,\text{crit}} = \frac{\pi^2 D_2 L_x}{(L_y/2)^2} \quad (4)$$

In this formula, the factor of 2 is a consequence of assuming deformation in a free bar of finite length, where the wavelength of the most unstable mode is twice the length of the bar. In our simulation, the wavelength corresponding to longitudinal instability is determined by periodicity conditions in the y-direction. For the cell with $N = 576$, shown in Figure 5, the
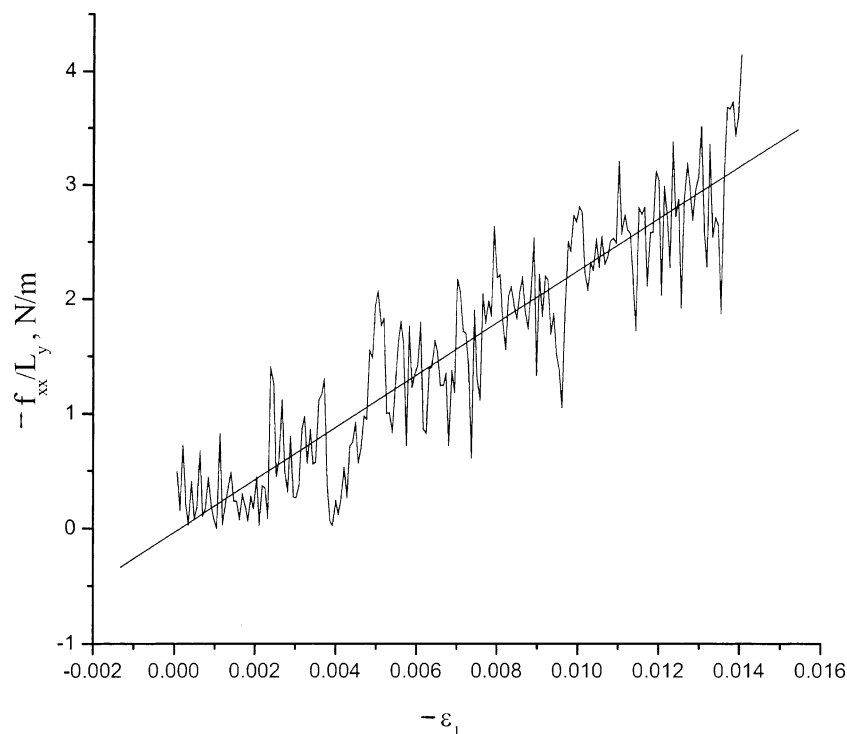
Figure 2. Force per unit length (f_{xx}/L_y) vs strain ϵ_1 (in the *x*-direction) during compression; $N = 288$.
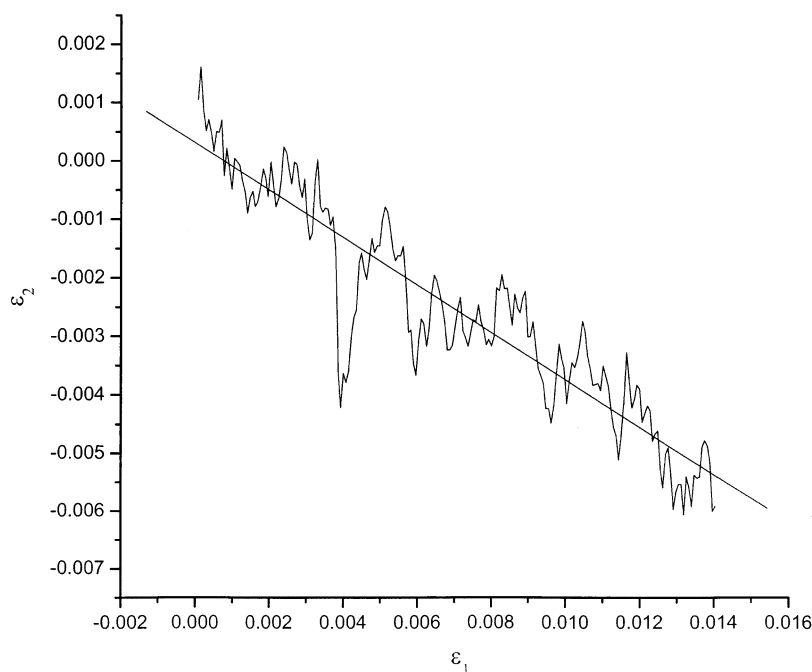

Figure 3. Strain ϵ_2 vs strain ϵ_1 during compression deformation in the *y*-direction; $N = 288$.

deformation becomes nonlinear at a compressive strain of $\epsilon_2 = -0.034$ (corresponding to a force per unit length of -8.73 N/m) indicative of the onset of an out-of-plane bending deformation. For the cell with $N = 864$ (i.e., L_y is 1.5 times larger), the deformation becomes nonlinear at $f_{yy}/L_x = -3.87$ N/m, in full agreement with the scaling suggested by eq 4. For the cell with $N = 288$, the deformation becomes nonlinear at $f_{yy}/L_x = -28.6$ N/m; the stress in this case is larger than that predicted by eq 4, which is a consequence of the very short wavelength of bending imposed by the smaller simulation cell. Such short wavelength bending requires significant distortion of the unit cell itself. From the observed values of f_{yy}/L_x and L_y for $N = 576$ and $N = 864$, we obtain consistently from eq 4 a value for

D_2 of 1.25×10^{-17} Nm, independent of the value assumed for sheet thickness.

4. Discussion

To our knowledge, experimental values for the elastic constants of MMT are not available for validation of the simulation results. The reported modulus for Al_2O_3 crystals is 530 GPa,[10] and experimental data for mica fibers yield a value of 230 GPa for the fiber modulus.[10] The full elastic stiffness matrix for bulk muscovite mica has been obtained by Brillouin scattering;[18] values for E_1, E_2, and E_3 are 159, 152, and 56 GPa, respectively. However, these results for bulk clays necessarily
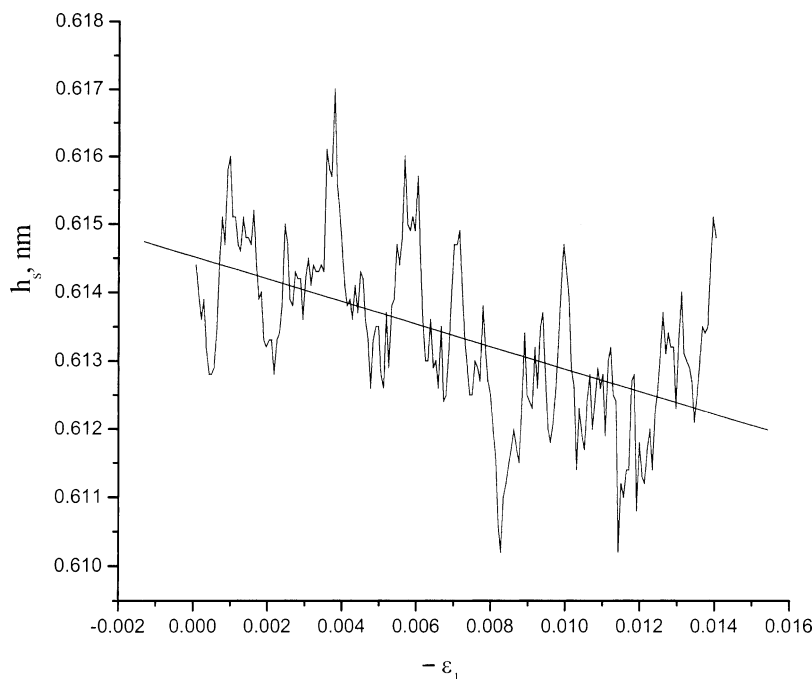
Elastic Properties of Montmorillonite

J. Phys. Chem. B, Vol. 108, No. 4, 2004 **1433**

Figure 4. Dependence on strain ϵ_1 of the distance h_s between planes of oxygen atoms at either surface of the clay layer for compression deformation in the *x*-direction; $N = 288$.
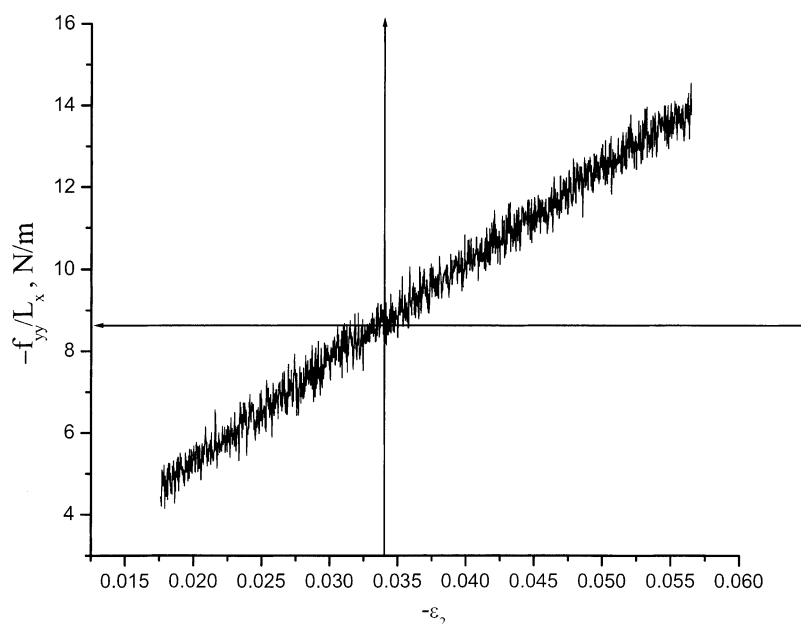

Figure 5. Force per unit length (f_{yy}/L_x) vs strain ϵ_2 (in the *y*-direction) during compression; $N = 576$.

include the contribution of the gallery spacing between clay lamella, across which only nonbonded interactions are operative. As a consequence, elastic constants estimated for bulk clays are certainly lower than those expected for the isolated lamella, because of the cross-sectional area of the nonload-bearing gallery (for in-plane elastic constants) and the easily deformed inter-lamellar separation (for elastic constants measured normal to the lamella).

To translate the results for atomistic deformation of an atomic body, reported in this work, into elastic constants characteristic of a macroscopic body and to compare the results to bulk measurements, it is necessary to specify the thickness *h* of the thin plate and to compare this with the periodic spacing between sheets in the bulk clay. From the viewpoint of atomic structure, the obvious choice for *h* of an isolated sheet is the average distance $h_s = 0.615$ nm found between opposing layers of oxygen atom centers at each surface of the sheet. This is consistent with the idea of atom-centered interactions, where loads may be carried only at the centers of atoms. This is about $^2/_3$ of the center-to-center distance between lamellae in the bulk material. Thus, one can also define a thickness $h_\rho = 0.96$ nm based on a typical bulk density of MMT of around 2.5 g/cm³. The difference between h_s and h_ρ can be rationalized in large part as the thickness of a region in the surrounding material excluded by the presence of a single clay sheet. For example, if one takes the surrounding material to be fully excluded from the van der Waals radii of the outermost oxygen layers, then one would estimate a thickness for the clay sheet of approximately 0.883 nm (corresponding to the 0.615 nm center-to-center distance between oxygen layers plus roughly twice the van der Waals radius of an oxygen atom, 0.134 nm). However, in fact the volume (or thickness) excluded by a clay
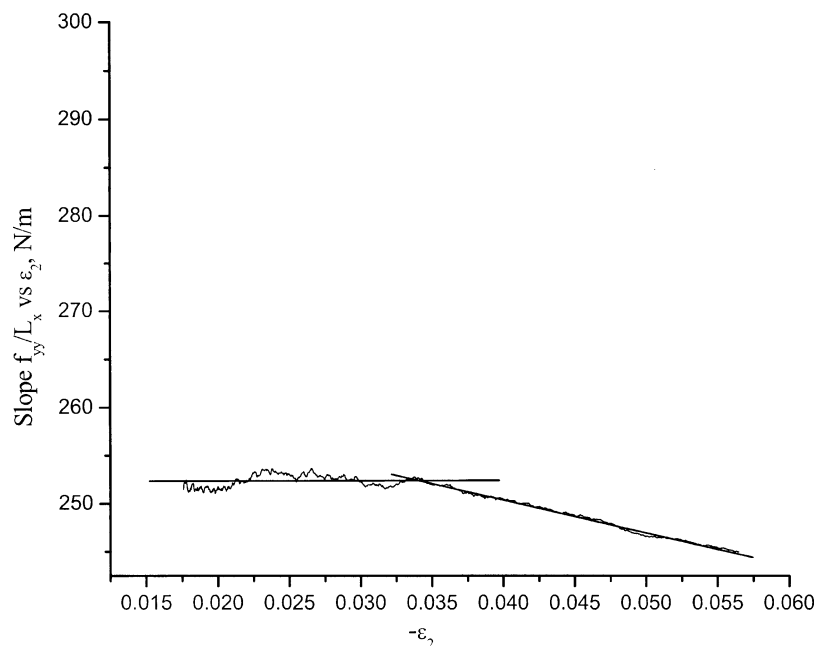
Figure 6. Slope $(\mathrm{d}f_{yy}/L_x/\mathrm{d}\epsilon_2)$ of the curve in Figure 5 vs strain ϵ_2 during compression in the *y*-direction, showing the change in slope due to yield in bending.

TABLE 3: Elastic Properties Determined Using Different Simulation Protocols[a]

elastic constants	$N = 288$ strain rate $= 1.5 \times 10^{-3}$ m/s	$N = 288$ strain rate $= 2.0 \times 10^{-4}$ m/s	$N = 48$ strain rate $= 1.5 \times 10^{-3}$ m/s
$E_1 h$ (N/m)	229	249	257
$E_2 h$ (N/m)	261	259	254
$E_3 h$ (N/m)	239	na	na
ν_{21}	0.41	0.44	0.45
ν_{12}	0.45	0.49	0.49
ν_{31}	0.27	0.18	0.08
ν_{32}	0.27	0.17	0.11
ν_{13}	0.14	na	na
ν_{23}	0.14	na	na
$G_1 h$ (N/m)	162	na	na
$G_2 h$ (N/m)	66.4	na	na
$G_3 h$ (N/m)	170	167	169
D_1/h^2 (N/m)	24.7	26.8	27.8
D_2/h^2 (N/m)	26.7	27.9	27.4
D_3/h^2 (N/m)	14.1	14.1	14.2

[a] Entries of "na" indicate "not applicable".

sheet in a surrounding matrix will vary depending on the strength of the interaction between the clay and the matrix. For the uncharged bulk clay, this interaction is relatively weak.

A third thickness for the sheet, the "effective mechanical thickness" h_m, can be defined using known relations from continuum mechanics of solids. For example, using the value for bending stiffness $D_2 = 1.25 \times 10^{-17}$ Nm obtained from the critical force for nonlinear deformation in compression simulations and $D_2/h^2 = 27.2$ N/m (cf. Table 3) computed from tensile deformation simulations and eq 3, one obtains $h_m = 0.678$ nm, in remarkable agreement with the value for h_s. A similar procedure has been used to estimate an effective wall thickness for carbon nanotubes; in that case, the effective wall thickness was only a fraction of the van der Waals radii of the atoms in the graphite sheet.[19]

Finally, the moduli for an isolated clay sheet obtained by simulation may be rationalized with the bulk values by making the relatively simple approximation of the bulk clay as a set of parallel alternating layers of clay sheets and galleries. Voigt averaging, $E_{\text{bulk}} = fE_{\text{sheet}} + (1 - f)E_{\text{gallery}}$, may then be used to estimate $E_{1,\text{bulk}}$ and $E_{2,\text{bulk}}$, where $f = h/L$. Here, L is the center-to-center distance between lamellae in the bulk material. Reuss

averaging may be used to estimate $E_{3,\text{bulk}}$. With the further approximation that $E_{i,\text{sheet}} \gg E_{i,\text{gallery}}$ for the in-plane moduli ($i = 1, 2$), one predicts a bulk modulus of roughly 270 GPa, independent of the definition of sheet thickness, h. This value for bulk modulus is in reasonable agreement with the observed value of 230 GPa for mica fibers cited earlier.[10] The lower experimental value is probably due to imperfections in crystallite orientation and nonuniform stress distribution in the real fiber. Furthermore, if one assumes an appropriate thickness of 0.615 nm for h, the resulting in-plane modulus for a single sheet of MMT is about 400 GPa, in reasonable agreement with values of modulus for bulk aluminosilicates such as stishovite ($E_1 = 453$ GPa[20]), whose density is 4.3 g/cm^3 and for which there is no gallery contribution.

5. Conclusion

We have studied the structure and elastic behavior of a single isolated sheet of MMT by molecular dynamics simulation. In the absence of applied deformation, the equilibrium structure of the clay sheet is in good agreement with the available X-ray diffraction data for MMT. This suggests that the force field

employed is adequate for this purpose. For slow rates of deformation and simulation cells of 288 atoms, we obtained results for elastic behavior that are independent of deformation rate and of system size, suggesting that these are indicative of the limiting behavior for an infinite clay sheet. The resulting values for elastic constants suggest that the clay layer may be represented approximately (within 10% error) as a sheet with orthotropic symmetry, having in-plane elastic properties $E_i h$ of $250-260$ N/m (E_1, $E_2 = 400-420$ GPa assuming $h = 0.615$ nm) and an out-of-plane elastic constant $E_3 h$ of 239 N/m ($E_3 = 390$ GPa assuming $h = 0.615$ nm). Bending stiffness D_2 was estimated independently to be 12.5×10^{-17} Nm, and the "effective mechanical thickness" was found to be comparable to the distance between planes of oxygen atoms at either surface of the clay sheet. Taken together, these results rationalize the connection between atomistic deformation and continuum models and substantiate in particular the use of the continuum mechanics of thin plates for single clay sheets of MMT.

References and Notes

(1) Pinnavaia, T. J.; Beall, G. W. *Polymer−Clay Nanocomposites*; John Wiley and Sons: Chichester, U.K., 2000.

(2) Grigoras, S.; Gusev, A. A.; Santos, S.; Suter, U. W. Evaluation of Elastic Constants of Nanoparticles from Atomistic Simulations. *Polymer* **2002**, *43* (2), 489.

(3) Shrol, R. M.; Smith, D. S. Molecular Dynamics Simulation in the Grand Canonical Ansemble. Application to Clay Minerals Swelling. *J. Chem. Phys.* **1999**, *111* (19), 9025.

(4) Ichikawa, Y.; Kawamura, K.; Nakano, M.; Kitayama, K.; Kawamura, H. *Eng. Geol.* **1999**, *54*, 21.

(5) Zaoni, A.; Sekkel, W. Molecular Dynamics Study of Mechanical and Thermodynamic Properties of Pentacrythritol Tetranite. *Solid State Commun.* **2001**, *118*, 345.

(6) Ledletter, H.; Kim, S.; Dann, M.; Xu, Z.; Crudele, S.; Kriven, W. Elastic Constants of Mullite Containing Alumina Platelets. *J. Eur. Ceram. Soc.* **2001**, *211*, 2567.

(7) Seo, Y. S.; Ichikawa, Y.; Kawamura, K. Stress−Strain Response of Rock-Forming Minerals by Molecular Dynamics Simulation. *Mater. Sci. Res. Int.* **1999**, *5*, 13.

(8) Sato, H.; Yamagishi, A.; Kawamura, K. Molecular Simulation for Flexibility of a Single Clay Layer. *J. Phys. Chem. B* **2001**, *105*, 7990.

(9) Brown, G. *The X-ray Identification and Crystal Structures of Clay Minerals*; Mineralogical Society: London, 1961.

(10) Kelly, A. *Strong Solids*; Clarendon Press: Oxford, U.K., 1973.

(11) Lemak, A. S.; Balabaev, N. K. *Mol. Simul.* **1994**, *13*, 177.

(12) *MSI, Insight II User Guide*, version 4.0.0; Molecular Simulations, Inc.: San Diego, CA, 1996.

(13) Allen, M. P.; Tildesley, D. J. *Computer Simulation of Liquids*; Clarendon Press: Oxford, U.K., 1987.

(14) Lemak, A. S.; Balabaev, N. K. A Comparison between Collisional Dynamics and Brownian Dynamics. *Mol. Simul.* **1995**, *15*, 223.

(15) Lemak, A. S.; Balabaev, N. K. Molecular Dynamics Simulation of Polymer Chain in Solution by Collisional Dynamics Method. *J. Comput. Chem.* **1996**, *17*, 1685.

(16) Berendsen, H. J. C.; Postma, P. J. P. M.; Van Gunsteren, W. F.; DiNola, A.; Haak, J. R. *J. Chem. Phys.* **1984**, *81*, 3684.

(17) Lekhnitskiy, S. G. *Anisotropic plates*; Gostehteorizdat: Moscow, 1957.

(18) McNeil, L. E.; Grimsditch, M. Elastic Moduli of Muscovite Mica. *J. Phys.: Condens. Matter* **1993**, *5*, 1681.

(19) Yakobbson, B. I.; Brabec, C. J.; Bernholc, J. *Phys. Rev. Lett.* **1996**, *75*, 2511.

(20) Sinclair, W.; Ringwood, A. E. *Nature (London)* **1978**, *78*, 714.